Biomacromolecules

pubs.acs.org/Biomac

Article

CXCR4-Mediated Codelivery of FLT3 and BCL-2 Inhibitors for Enhanced Targeted Combination Therapy of FLT3-ITD Acute Myeloid Leukemia

Jiakun Yang, Peng Zhang, Yumin Mao, Ran Chen, Ru Cheng,* Jiaying Li, Huanli Sun,* Chao Deng, and Zhiyuan Zhong*

Cite This: *Biomacromolecules* 2024, 25, 4569−4580

Read Online

ACCESS | Metrics & More | Article Recommendations | Supporting Information

ABSTRACT: Acute myeloid leukemia (AML) is often associated with poor prognosis and survival. Small molecule inhibitors, though widening the treatment landscape, have limited monotherapy efficacy. The combination therapy, however, shows suboptimal clinical outcomes due to low bioavailability, overlapping systemic toxicity and drug resistance. Here, we report that CXCR4-mediated codelivery of the BCL-2 inhibitor venetoclax (VEN) and the FLT3 inhibitor sorafenib (SOR) via T22 peptide-tagged disulfide cross-linked polymeric micelles (TM) achieves synergistic treatment of FLT3-ITD AML. TM-VS with a VEN/SOR weight ratio of 1/4 and T22 peptide density of 20% exhibited an extraordinary inhibitory effect on CXCR4-overexpressing MV4−11 AML cells. TM-VS at a VEN/SOR dosage of 2.5/10 mg/kg remarkably reduced leukemia burden, prolonged mouse survival, and impeded bone loss in orthotopic MV4−11-bearing mice, outperforming the nontargeted M-VS and oral administration of free VEN/SOR. CXCR4-mediated codelivery of BCL-2 and FLT3 inhibitors has emerged as a prospective clinical treatment for FLT3-ITD AML.

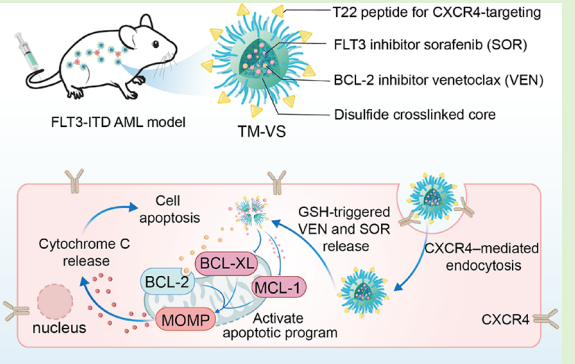

1. INTRODUCTION

Acute myeloid leukemia (AML) is a highly aggressive and heterogeneous myeloid cancer diagnosed mainly in elderly people and is associated with poor prognosis.[1−3] Cytarabine and daunorubicin-based standard chemotherapy, though improving the survival of eligible younger patients, is perplexing with high systemic toxicity, making most elderly patients ineligible, with a 5 year survival rate below 10%.[4−6] With an improved understanding of AML genomics, several important molecular targets influencing prognosis and treatment decisions have been identified.[7−9] Mutations in FMS-like tyrosine kinase 3 (FLT3), including FLT3 internal tandem duplications (FLT3-ITD) and the FLT3 tyrosine kinase domain (FLT3-TKD), are most frequently detected in AML patients (∼30%) and are correlated with an inferior prognosis compared to wild-type FLT3 AML.[10−12] Recent approval of FLT3 inhibitors, such as midostaurin, sorafenib (SOR) and gilteritinib, has altered the treatment landscape for FLT3 mutant AML patients.[13,14] However, due to the emergence of drug resistance, FLT3 inhibitors generally have limited monotherapy efficacy and are often administered in combination with chemotherapeutics or other small molecular targeted drugs, such as B-cell lymphoma-2 (BCL-2) inhibitors.[15]

BCL-2 is an antiapoptotic protein that is overexpressed in AML cells and promotes leukemic blast survival through regulation of the mitochondrial apoptotic pathway.[16] Venetoclax (VEN), a highly selective BCL-2 inhibitor, in combination with hypomethylating agents or low-dose cytarabine has been approved as a standard option for newly diagnosed AML patients who are unfit for intensive chemotherapy.[17−19] Recent studies have indicated the synergistic effect of VEN in combination with FLT3 inhibitors in FLT3-ITD AML models,[20,21] likely due to the simultaneous downregulation of MCL-1 and BCL-XL antiapoptotic proteins, which can facilitate VEN resistance.[22,23] Moreover, early phase clinical trials have shown encouraging response rates and survival benefits in FLT3 mutant AML patients after combination therapy with VEN and FLT3 inhibitors.[24−26] Nevertheless, this combination is associated with poor bioavailability, dose-dependent myelosuppression, overlapping systemic toxicity, and drug resistance, limiting its clinical benefits.

Received: April 25, 2024
Revised: May 31, 2024
Accepted: June 4, 2024
Published: June 13, 2024

https://doi.org/10.1021/acs.biomac.4c00561
Biomacromolecules 2024, 25, 4569−4580

Herein, T22 peptide-modified disulfide cross-linked polymeric micelles (TM) were engineered to enable C-X-C motif chemokine receptor 4 (CXCR4)-mediated codelivery of BCL-2 (VEN) and FLT3 (SOR) inhibitors for safe and synergistic treatment of FLT3-ITD AML (Scheme 1). CXCR4 is overexpressed in leukemia cells of most AML patients and is correlated with drug resistance and decreased survival.[27−30] The T22 peptide, which is an engineered version of the polyphemusin II peptide from the horseshoe crab and has high affinity for CXCR4,[31,32] was introduced to the surface of micelles to target AML. VEN and SOR coloaded micelles (TM-VS) were prepared with efficacious VEN/SOR loading, a tailored VEN/SOR ratio, high stability, and reduction responsive drug release. Intriguingly, TM-VS treatment markedly reduced leukemia burden in the bone marrow, blood system, and main organs, prolonged mouse survival, and impeded bone loss in orthotopic MV4−11 FLT3-ITD AML-bearing mice, outperforming all the other controls. Moreover, compared with oral administration of free VEN/SOR at doses of 150 and 30 mg/kg, TM-VS induced minimal myelosuppression and reduced damage to blood cells and major organs. TM-VS has emerged as a safe and effective dual-molecular targeting nanoinhibitor for combination therapy of FLT3 mutant AML.

Scheme 1. T22 Peptide-Tagged Disulfide Cross-linked Polymeric Micelles for CXCR4-Mediated Codelivery of VEN and SOR to Enable Synergistic Treatment of Orthotopic MV4-11 AML-Bearing Mice

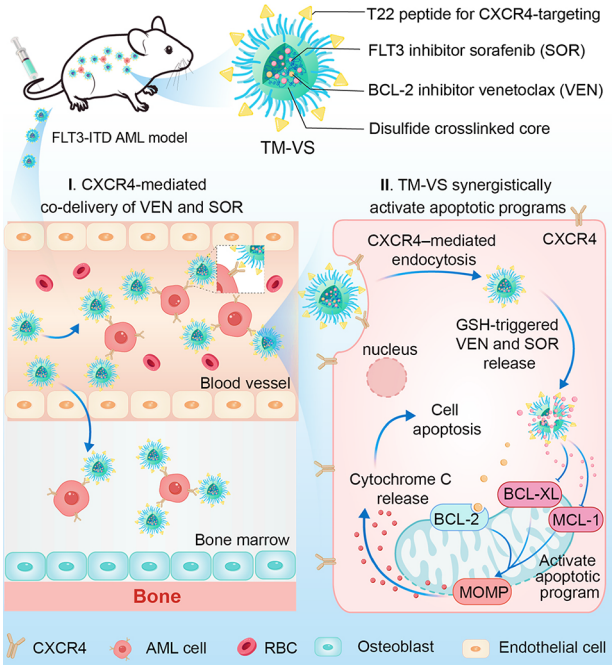

2. EXPERIMENTAL SECTION

2.1. Preparation and Characterization of T22 Peptide-Modified VEN and SOR Coloaded Micelles (TM-VS). TM-VS was prepared via coassembly of T22 peptide-functionalized poly(ethylene glycol)-*b*-poly(ε-caprolactone-*co*-dithiolane trimethylene carbonate) (T22-PEG-*b*-P(CL-*co*-DTC)) and PEG-*b*-P(CL-*co*-DTC) copolymers at a weight ratio of 1/4 with simultaneous VEN and SOR loading. By adjusting the VEN/SOR weight ratio (*x*), TM-VS$_x$ with different T22 surface densities and VEN/SOR ratios could be obtained. Taking TM-VS$_{1/4}$ as an example, 100 μL of polymer solution in *N*,*N*-dimethylformamide (DMF) (10 mg/mL) with 20% T22-PEG-*b*-P(CL-*co*-DTC) was mixed with 1 μL of VEN and 5 μL of SOR solution in DMF (10 mg/mL) and then injected into 900 μL of phosphate buffer (PB, pH 7.4, 10 mM) under stirring. The suspension was dialyzed (MWCO: 3.5 kDa) against PB for 6 h to afford T$_{20}$M-VS$_{1/4}$. Nontargeted M-VS, M-V, and M-S were prepared via self-assembly of PEG-*b*-P(CL-*co*-DTC) only. The contents of VEN and SOR loaded in micelles were measured by high-performance liquid chromatography (HPLC) after overnight incubation with 10-fold acetonitrile with excess dithiothreitol. The drug loading content (DLC) and drug loading efficiency (DLE) were calculated according to the following formulas:

$$\mathrm{DLC(wt.\ \%)} = \text{weight of loaded drug} / \text{weight of polymers and loaded drug} \times 100$$

$$\mathrm{DLE(\%)} = \text{weight of loaded drug} / \text{weight of drug in feed} \times 100$$

The morphology of TM-VS was observed by transmission electron microscopy (TEM). The self-cross-linking of the micelles was verified by UV−vis spectrophotometry. The stability of TM-VS after storage at 4 °C for 20 days, incubation in 10% fetal bovine serum (FBS) for 24 h, 100-fold dilution with PB, or incubation with 10 mM GSH was determined by dynamic light scattering (DLS). To confirm the reduction-triggered release of VEN and SOR, TM-VS and that incubated with 10 mM GSH for 12 h were subjected to HPLC measurements.

2.2. CXCR4 Levels in AML Cell Lines. To evaluate the CXCR4 expression level in different AML cell lines (MV4−11, MOLM-13-Luc, HL-60, and OCI-AML3), 1 × 10^6 cells were suspended in 200 μL of PBS and incubated with 2 μL of APC-conjugated anti-CXCR4 antibody for 30 min in the dark at room temperature. Then, the cells were washed twice and resuspended in 200 μL of PBS for flow cytometry analysis.

2.3. In Vitro Cellular Uptake and Targetability of TM-VS. T$_y$M-Cy5 (*y*: 10, 20, and 30, the weight percentage of the T22-PEG-*b*-P(CL-*co*-DTC) copolymer) and M-Cy5 were engineered to monitor the cellular uptake of TM-VS in four types of AML cells (MV4−11, MOLM-13-Luc, HL-60, and OCI-AML3) via flow cytometry and confocal laser scanning microscopy (CLSM). For flow cytometry studies, cells seeded in 6-well plates (2 × 10^5/well) were cultured for 4 h with 200 μL of T$_y$M-Cy5 (*y*: 10, 20, or 30), M-Cy5, or PBS at 37 °C with a final Cy5 concentration of 2.0 μg/mL. Afterward, the cells were collected by centrifugation (1000 rpm, 4 min), washed with PBS, and resuspended in 200 μL of PBS for immediate flow cytometry analysis. At least 1 × 10^4 cells were counted, and the data were analyzed using FlowJo-10 software. To corroborate the CXCR4-mediated endocytosis of TM-VS, MV4−11 and MOLM-13-Luc cells were pretreated with 10 μM free T22 peptide for 2 h at 37 °C prior to incubation with T$_{20}$M-Cy5 followed by a similar procedure for flow cytometry analysis.

2.4. In Vitro Anti-AML Studies. The synergistic anti-AML effect of M-VS at different VEN/SOR ratios in MV4−11 and MOLM-13-Luc cells was first assessed by a CCK-8 assay. Cells were seeded in 96-well plates (2 × 10^4 cells/well) and treated with M-VS (V/S: 1/1, 1/2, 1/4 or 1/6, w/w), M-V, or M-S at various drug concentrations. After 48 h of incubation, 10 μL of CCK-8 solution was added for another 3 h of incubation. The absorbance at 450 nm was detected by a microplate reader. Cell viability was determined by comparing the absorbance of cells treated with different samples with that of PBS-treated cells (n = 6). The anti-AML effect of M-VS with VEN/SOR ratios (w/w) of 2/1, 4.8/1, and 5.8/1 in MV4−11 cells was evaluated similarly. The combination index (CI) was calculated according to Chou and Talalay's method.[33]

$$\mathrm{CI} = \frac{C_V}{S_V} + \frac{C_S}{S_S}$$

https://doi.org/10.1021/acs.biomac.4c00561
Biomacromolecules 2024, 25, 4569−4580

where S_V and S_S represent the half maximal inhibitory concentration (IC_{50}) values of M-V and M-S, respectively. C_V and C_S are the IC_{50} values of VEN and SOR in M-VS, respectively. CI < 1, CI = 1, and CI > 1 indicate synergistic, additive, and antagonistic effects, respectively. The CI-Fa (fraction affected) curves were fitted by Compusyn software (Fa: fraction affected rate, 0−1).

After confirmation of the synergistic effect of M-VS, the *in vitro* anti-AML activity of T_{20}M-VS was further studied using nontargeted M-VS and free VS as controls. T_{20}M-$VS_{1/4}$, M-$VS_{1/4}$, and free $VS_{1/4}$ (SOR: 0.01−30 ng/mL) were evaluated in MV4−11 cells, and T_{20}M-$VS_{1/2}$, M-$VS_{1/2}$, and free $VS_{1/2}$ (SOR: 0.001−2.5 ng/mL) were assessed in MOLM-13-Luc cells (n = 4).

The cytotoxicity of T_{20}M-$VS_{1/4}$ and M-$VS_{1/4}$ (SOR: 0.1−1000 ng/mL) toward peripheral blood mononuclear cells (PBMCs, 5×10^5 cells/well), DC 2.4 and L929 cells (5×10^3 cells/well) was assessed similarly using a CCK-8 assay (n = 5). The cytotoxicity of blank micelles (T_{20}M and M) toward MV4−11 and MOLM-13-Luc cells was also evaluated similarly with micelle concentrations ranging from 1 to 400 μg/mL (n = 4).

2.5. Western Blot Analysis. Western blotting was used to investigate the influence of different drug formulations on antiapoptotic proteins in MV4−11 and MOLM-13-Luc cells. Cells in 6-well plates (1×10^6 cells/well) were incubated for 48 h with T_{20}M-VS, M-VS, free VS, M-V, or M-S. The VEN and SOR concentrations were set at 2 and 8 ng/mL for the MV4−11 cells and 1 and 2 ng/mL for the MOLM-13-Luc cells, respectively. After incubation, the cells were lysed using ice-cold RIPA buffer for 30 min and centrifuged at 12000 rpm and 4 °C. The protein in the supernatant was quantified, and 20 μg of protein from each sample was mixed with bromophenol blue solution, boiled for 10 min, and separated by 10% SDS−PAGE. The proteins were then transferred to a poly(vinylidene difluoride) membrane, which was blocked with 5% skim milk at 25 °C for 1.5 h and incubated overnight with BCL-2, MCL-1, and BCL-XL antibodies or β-actin antibodies at 4 °C. After washing with Tris-buffered saline/0.1% Tween-20 (TBST), the membrane was incubated with horseradish catalase-labeled secondary antibody for 1.5 h at room temperature and washed with TBST to acquire images using an electrochemiluminescence detection system (Pierce).

2.6. Cell Apoptosis and Mitochondrial Membrane Permeability. The pro-apoptotic activity of different formulations (M-V, M-S, free VS, M-$VS_{1/4}$, and T_{20}M-$VS_{1/4}$) in MV4−11 and MOLM-13-Luc cells was investigated using an Annexin V-APC and 7-amino-actinomycin D (7-AAD) apoptosis detection kit. Cells seeded in 12-well plates (2×10^5 cells/well) were treated with different formulations (VEN/SOR: 2/8 ng/mL for MV4−11 cells, 1/2 ng/mL for MOLM-13-Luc cells) for 48 h. Then, the cells were harvested, washed twice with cold PBS, and resuspended in 300 μL of binding buffer followed by 5 min of staining with 5 μL of Annexin V-APC and 10 μL of 7-AAD at 25 °C. Flow cytometry measurements were performed immediately, and at least 2×10^4 cells were analyzed per sample. Cells treated with PBS only and those treated with apoptosis-positive control solution were used as negative and positive controls, respectively.

To study the influence of different formulations on mitochondrial membrane permeability, MOLM-13-Luc and MV4−11 cells seeded in 6-well plates (5×10^5 cells/well) were incubated with T_{20}M-VS, M-VS, free VS, M-V, or M-S for 48 h. The drug concentrations were the same as those used in the apoptosis studies. After removing the culture medium, the cells were treated with JC-1 at 37 °C for 20 min according to the manufacturer's instructions for the mitochondrial membrane potential assay kit. The percentage of cells with red and green fluorescence was analyzed by flow cytometry using PE and FITC channels.

2.7. In Vivo Acute Toxicity Experiments. All animal procedures were handled under protocols approved by the Soochow University Laboratory Animal Center and the Animal Care and Use Committee of Soochow University. The acute toxicity of TM-VS and free VS *in vivo* was evaluated by using female BALB/c mice (n = 4). PBS was used as a control. T_{20}M-VS at 2.5/10 mg V/S equiv/kg was administered intravenously every 2 days for a total of 4 injections. Free VS (150/30 mg/kg) was administered every day by oral gavage for 7 days as previously reported.[22] The body weight and health status of the mice were continuously monitored for 8 days. On day 9 after drug administration, blood was collected from the abdominal cavity of the mice in each group for routine blood and blood biochemistry analyses.

2.8. Ex Vivo Imaging. To assess the targetability and biodistribution of different formulations, an orthotopic MV4−11 model was established by intravenous transplantation of 200 μL of MV4−11 cells (5×10^5 cells per mouse) via the tail vein into B-NDG mice (female, 8 weeks, 19−22 g). On day 20 after tumor inoculation, a single dose of T_{20}M-Cy5 or M-Cy5 (Cy5:0.5 μg per mouse, n = 3) in PBS (200 μL) was intravenously injected via the tail vein. After 8 h, the mice were sacrificed, and the major organs and limb bones were isolated and *ex vivo* imaged on an IVIS imaging system using Living Image 2.6 software.

2.9. In Vivo Anti-AML Efficacy in an Orthotopic MV4−11 AML Model. On day 3 after inoculation, orthotopic MV4−11 AML-bearing mice were randomly divided into 9 groups (n = 9) and treated with different formulations. TM-$VS_{1.25/5}$, M-$VS_{1.25/5}$, M-$V_{1.25}$, M-S_5, and free $VS_{1.25/5}$ at V/S dosages of 1.25/5 mg/kg, TM-$VS_{2.5/10}$ at V/S dosages of 2.5/10 mg/kg, TM-$VS_{10/10}$ at V/S dosages of 10/10 mg/kg and PBS were intravenously administered via the tail vein every 3 days for a total of 10 injections. The free VS (*p.o.*) group was given at V/S doses of 150/30 mg/kg every day via a gavage needle for two cycles, with five administrations in each cycle and a 10 day break before the second cycle.[22] The V/S dosages of intravenously injected formulations were determined based on the oral bioavailability of SOR (30−40%) and the in vitro synergistic ratio of M-VS (e.g., V/S 1:4). The mice were weighed, and the weights were recorded every 2 days. On day 32 after model establishment, 3 mice from each group were randomly sacrificed, and blood, hind limbs, and major organs were collected for routine blood analysis, blood biochemistry, and leukemia burden analysis. Three mice in the PBS group were sacrificed on day 20 to monitor the leukemia burden and make comparisons. Single-cell suspensions of blood and different tissues in PBS (containing 1% v/v FBS) were treated with red blood cell lysis buffer solution for 10 min. Then, the cells were stained with an APC-conjugated anti-CD45 antibody for 15 min and measured by flow cytometry. A total of 2×10^4 cells were analyzed per sample. The major organs as well as the tibia and femur of one mouse from each group were stained with hematoxylin and eosin (H&E) for histological analysis. The tibia and femur were also stained with a tartrate-resistant acid phosphatase (TRAP) kit to identify osteoclasts. To observe the bone structure, the femur and tibia were scanned by micro-CT (SkyScan 1176, Belguim). The reconstructed images and relevant parameters were analyzed by NRecon, DataViewer, and CTAn software. The other five mice were used for monitoring the survival rate.

2.10. Statistical Analysis. The data are presented as the means ± standard deviations (SDs). Significant differences among groups were determined using GraphPad Prism 8 by two-tailed Student's t test or one-way ANOVA. For bioinformatics analysis, the statistical significance was assessed by the Wilcoxon test. For survival analysis, the log-rank (Mantel−Cox) test was applied. Statistical significance was defined as $^*p < 0.05$, $^{**}p < 0.01$, $^{***}p < 0.001$, and $^{****}p < 0.0001$.

3. RESULTS AND DISCUSSION

3.1. Preparation and Characterization of TM-VS. To engineer TM-VS, PEG-*b*-P(CL-*co*-DTC) (5.0-(4.2−2.0) kg/mol, M_w/M_n = 1.1) and NHS-PEG-*b*-P(CL-*co*-DTC) (5.0-(3.7−1.9) kg/mol, M_w/M_n = 1.2) were first synthesized via ring-opening copolymerization of ε-CL and DTC using mPEG−OH and NHS-PEG−OH as macroinitiators, respectively (Figure S1 and Table S1), similar to our previous report.[34] T22-PEG-*b*-P(CL-*co*-DTC) was constructed by amidation of NHS-PEG-*b*-P(CL-*co*-DTC) with DBCO-NH_2

https://doi.org/10.1021/acs.biomac.4c00561
Biomacromolecules 2024, 25, 4569−4580

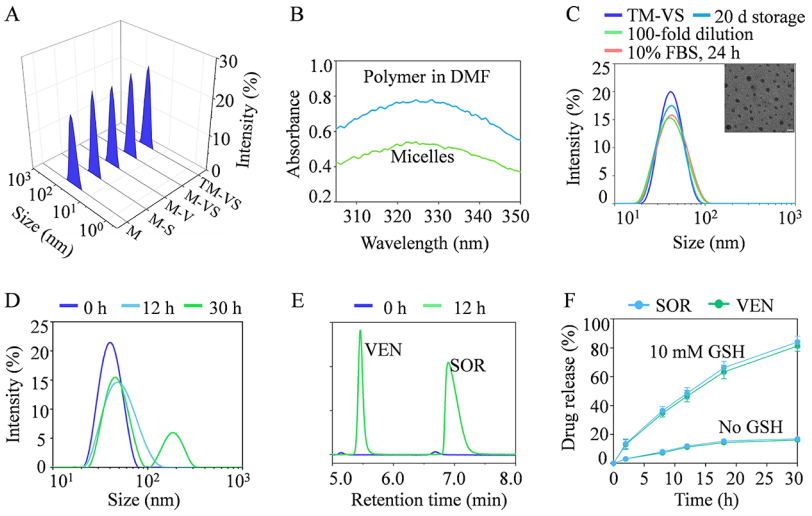

Figure 1. Characterization of TM-VS. (A) Size distribution of M, M-S, M-V, M-VS, and TM-VS determined by DLS. (B) UV absorbance of a PEG-*b*-P(CL-*co*-DTC) solution in DMF and after assembly in PB (pH 7.4, 10 mM). (C) Stability of TM-VS$_{1/4}$ at 1.0 mg/mL after 20 days of storage at 4 °C, 100-fold dilution or 10% FBS at 37 °C. Insert: TEM image of TM-VS$_{1/4}$. Scale bar: 50 nm. (D) Changes in the size of TM-VS$_{1/4}$ in response to 10 mM GSH at 37 °C. (E) HPLC chromatograms of TM-VS$_{1/4}$ before or after treatment with 10 mM GSH for 12 h. (F) *In vitro* VEN or SOR release profiles from TM-VS$_{1/4}$ at 37 °C with or without 10 mM GSH (n = 3).

Table 1. Characterization of M-VS and TM-VS with Different VEN/SOR Ratios

		VEN/SOR				
		DLC (*wt.*%)				
entry	formulation	theo.	deter.[a]	DLE (%)[a]	size (nm)[b]	PDI[b]
1	M-VS$_{1/1}$	5.0/5.0	3.9/4.1	76/80	40.2 ± 0.5	0.05 ± 0.01
2	M-VS$_{1/2}$	2.0/5.0	1.7/3.9	84/76	39.0 ± 0.8	0.07 ± 0.03
3	M-VS$_{1/4}$	1.0/5.0	1.0/4.0	99/78	38.9 ± 0.6	0.07 ± 0.01
4	M-VS$_{1/6}$	0.7/5.0	0.7/4.2	99/82	38.6 ± 0.3	0.04 ± 0.01
5	TM-VS$_{1/1}$	5.0/5.0	4.4/4.3	86/84	40.1 ± 0.7	0.06 ± 0.02
6	TM-VS$_{1/2}$	2.0/5.0	1.9/3.9	97/76	40.2 ± 0.5	0.04 ± 0.01
7	TM-VS$_{1/4}$	1.0/5.0	1.0/4.0	99/78	39.8 ± 0.8	0.05 ± 0.02

[a]Determined by HPLC. [b]Measured by DLS (1.0 mg/mL, 25 °C).

and subsequent click reaction with azide-functionalized T22 peptide (T22-N$_3$) (Figure S1B). The ^{1}H NMR spectra confirmed the successful synthesis of T22-PEG-*b*-P(CL-*co*-DTC), which showed signals characteristic of the T22 peptide at δ 1.50, 2.60−3.20, 3.74, 4.20, 6.60, and 6.87−7.72 (Figure S2). The T22 functionality was 88.2%, as determined by a BCA protein assay kit.

TM-VS was prepared via coassembly of T22-PEG-*b*-P(CL-*co*-DTC) and PEG-*b*-P(CL-*co*-DTC) at a weight ratio of 1/4 with simultaneous VEN and SOR loading via hydrophobic interactions (Scheme S1). TM-VS bearing different VEN/SOR weight ratios (1/1, 1/2, 1/4) had a small size of ca. 40 nm and a uniform dispersion (PDI < 0.1), which was similar to that of nontargeted M-VS, single inhibitor-loaded micelles (M-V, M-S) and blank micelles (Figure 1A, Table 1, and Table S2). Notably, both TM-VS and M-VS displayed high loading efficiencies for VEN (DLE: 76−99%) and SOR (DLE: 76−84%), with VEN coloading enhancing the DLE of SOR in comparison to M-S (~60%), likely due to $\pi-\pi$ stacking between VEN and SOR (Table 1 and Table S2). Moreover, the DLE of SOR in TM-VS was superior to that of other SOR-loaded nanoparticles, with DLEs ranging from 20 to 60%.[35−37]

As shown in Figure 1B, the UV absorbance of the PEG-*b*-P(CL-*co*-DTC) polymers at 330 nm decreased obviously after assembly into micelles, demonstrating the self-cross-linking of the micelles by ring-opening polymerization of the dithiolane rings. The TEM image showed that TM-VS had a spherical structure (Figure 1C, inset). Similar to other disulfide-cross-linked nanomedicines,[38,39] TM-VS has good stability, maintaining its size and size distribution after incubation with 10% FBS for 24 h, storage at 4 °C for 20 days, or 100-fold dilution with PB (Figure 1C). In contrast, TM-VS displayed apparent destruction upon treatment with 10 mM GSH (Figure 1D) and consequently released both VEN and SOR in their native forms (Figure 1E). *In vitro* drug release data further revealed that TM-VS leaked approximately 16% of the VEN or SOR under physiological conditions, while more than 80% of the VEN and SOR were released in 12 h upon treatment with 10 mM GSH (Figure 1F). Interestingly, the release profiles of VEN and SOR were almost the same, which is important for maintaining the optimal intracellular drug ratio.

3.2. Cellular Uptake of TM-VS in AML Cell Lines.

CXCR4 is an important molecule involved in the spread and progression of AML and is a marker for poor prognosis.[40] Bioinformatics analysis of data from The Cancer Genome Atlas (TCGA) and Genotype-Tissue Expression (GTEx) databases revealed that the survival rate of AML patients with high CXCR4 expression (n = 31) was significantly lower than that of AML patients with low CXCR4 expression (n = 101) (*p = 0.032, Figure 2A). The CXCR4 expression levels in 4 kinds of

https://doi.org/10.1021/acs.biomac.4c00561
Biomacromolecules 2024, 25, 4569−4580

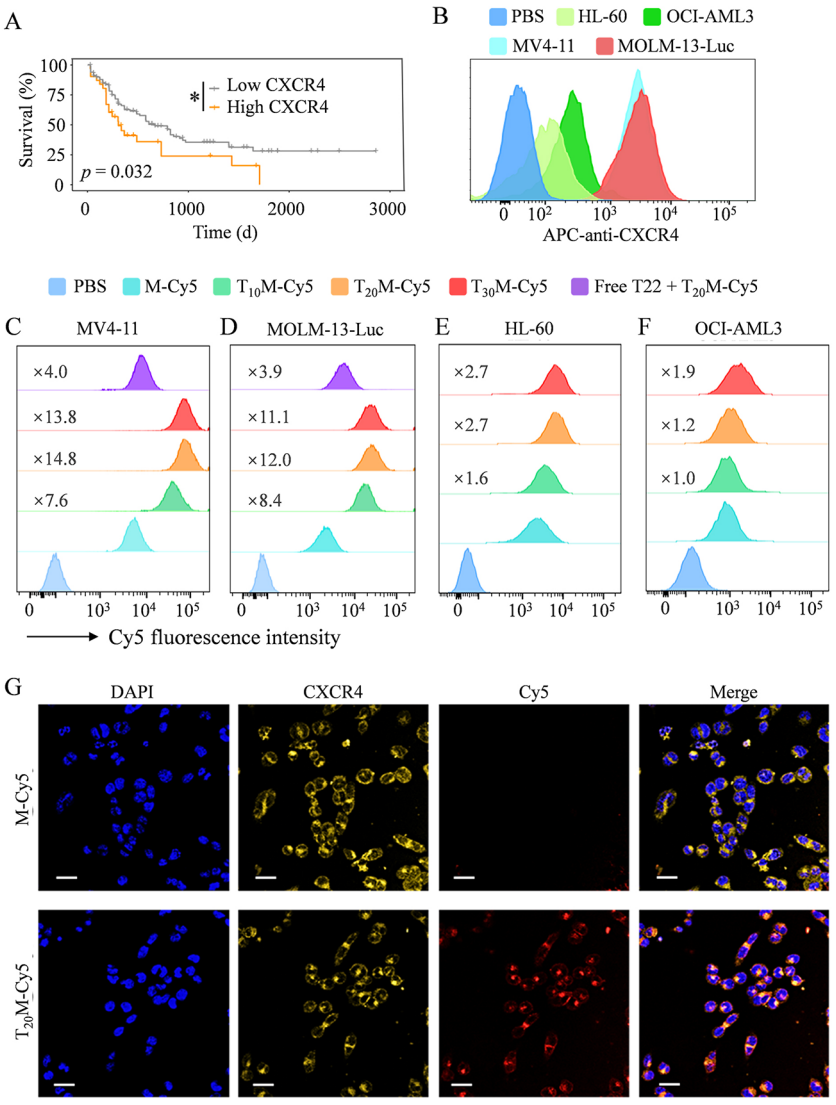

Figure 2. CXCR4 expression and cellular uptake studies. (A) Survival curve of AML patients with high or low CXCR4 expression. (B) CXCR4 levels on the surface of four AML cell lines. Cy5 fluorescence histograms of (C) MV4−11, (D) MOLM-13-Luc, (E) HL-60, and (F) OCI-AML3 cells following 4 h of incubation with T_xM-Cy5, M-Cy5, or PBS. The Cy5 fluorescence histograms of free T22 peptide-pretreated MV4−11 and MOLM-13-Luc cells following 4 h of incubation with T_{20}M-Cy5 are also shown in C or D. (G) CLSM images of MV4−11 cells after 4 h of incubation with M-Cy5 or T_{20}M-Cy5. Scale bars: 20 μm.

AML cells were measured by flow cytometry using an APC-conjugated anti-CXCR4 antibody. As shown in Figure 2B, CXCR4 was highly expressed in MV4−11 and MOLM-13-Luc cells, for which the CXCR4 level was over 22.5- and 11.1-fold higher than that in HL-60 and OCI-AML3 cells, respectively.

The cellular uptake of Cy5-labeled micelles was evaluated in MV4−11, MOLM-13-Luc, OCI-AML3, and HL-60 AML cells with different CXCR4 levels. In MV4−11 and MOLM-13-Luc AML cells with high CXCR4 expression, the cellular internalization of T_yM-Cy5 (y: 10, 20, and 30) was clearly greater than that of M-Cy5 (Figure 2C,D). T_{20}M-Cy5 had the best targetability in both the MV4−11 and MOLM-13-Luc cells, which exhibited 13.8-fold and 11.0-fold greater Cy5 fluorescence, respectively, than M-Cy5-treated cells. In HL-60 and OCI-AML3 cells with relatively low CXCR4 levels, TM-Cy5, which has different T22 contents, exhibited a 1.0- to 2.7-fold greater cellular uptake than M-Cy5 (Figure 2E,F). Furthermore, the cellular uptake of T_{20}M-Cy5 in MV4−11 and MOLM-13-Luc cells significantly decreased when the cells were pretreated with free T22 peptide (Figure 2C,D), indicating a CXCR4-mediated endocytosis pathway for TM. In line with the flow cytometry results, CLSM images showed that the Cy5 fluorescence in the MV4−11 cells incubated with T_{20}M-Cy5 was much stronger than that in the MV4−11 cells incubated with M-Cy5 (Figure 2G). In addition, some of the CXCR4 and Cy5 fluorescence signals overlapped, supporting the binding of TM-Cy5 to CXCR4. In the following studies, T_{20}M containing the optimal T22 density (20%) was used and denoted as TM.

3.3. In Vitro Synergistic Anti-AML Effect of TM-VS.

The anti-AML efficacy of M-VS at different drug ratios was first evaluated using a CCK-8 kit to determine the optimal VEN/SOR weight ratio. The results showed that M-VS with a VEN/SOR weight ratio of 1/1, 1/2, 1/4, or 1/6 had significantly greater anti-AML activity toward MV4−11 cells than M-V and M-S, leading to low CI values of 0.27−0.71 (Figure 3A and Table 2). With a further increase of VEN/SOR weight ratio to 2/1, 4.8/1, and 5.8/1, the CI values increased

https://doi.org/10.1021/acs.biomac.4c00561
Biomacromolecules 2024, 25, 4569−4580

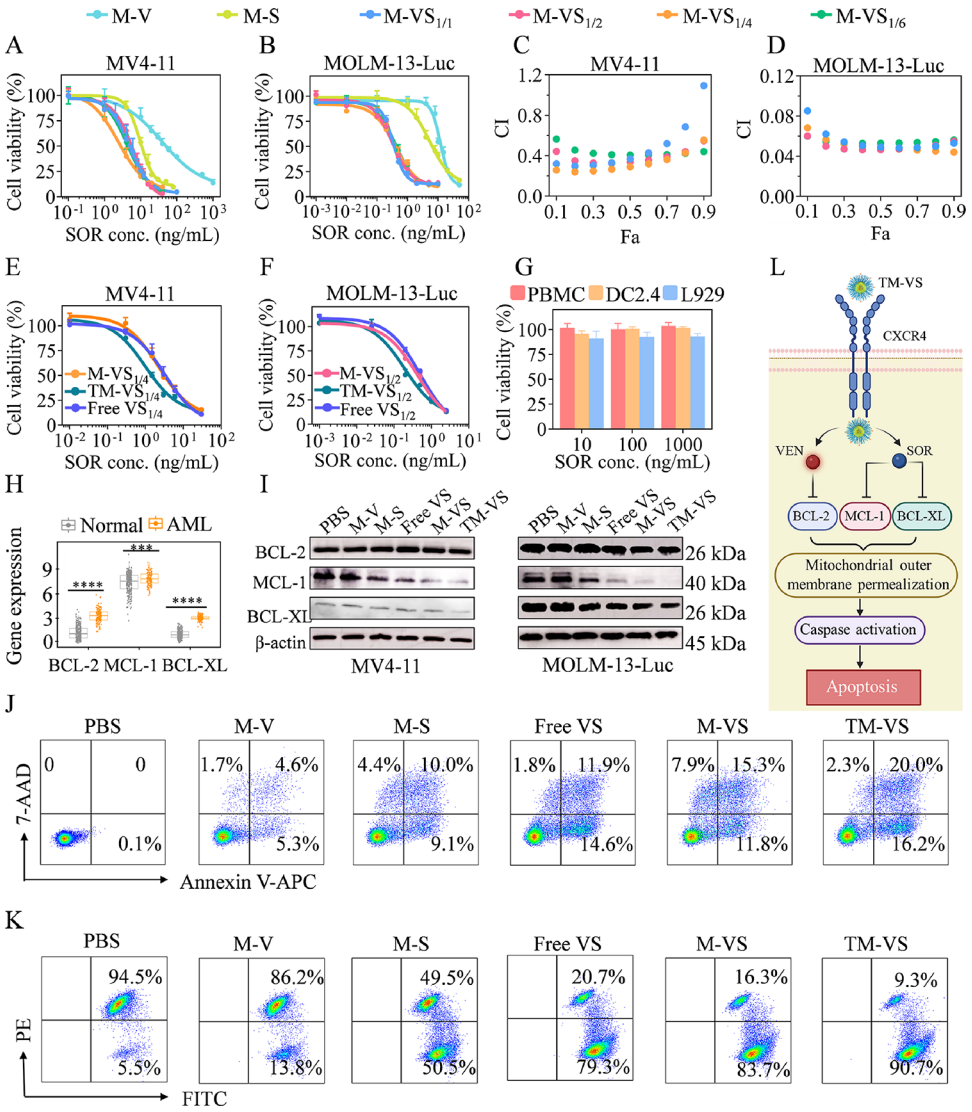

Figure 3. Cytotoxicity and apoptosis studies. Cell viability of (A) MV4−11 and (B) MOLM-13-Luc cells treated with M-V, M-S and M-VS at different VS ratios (V/S = 1/1, 1/2, 1/4, and 1/6 (w/w)) for 48 h (n = 6). The synergism of VEN and SOR in (C) MV4−11 and (D) MOLM-13-Luc cells was evaluated with CI-Fa values by CompuSyn software. The cytotoxicity of free VS, M-VS and TM-VS against (E) MV4−11 and (F) MOLM-13-Luc cells after 48 h of incubation (n = 4). (G) Cytotoxicity of TM-$VS_{1/4}$ against PBMCs, DC 2.4 cells and L929 cells (n = 5). (H) Expression of BCL-2, MCL-1, and BCL-XL genes in AML patients (n = 152) and healthy people (n = 337) isolated from TCGA and GTEx. (I) Protein expression in MV4−11 and MOLM-13-Luc cells after treatment with different formulations. The apoptosis of MV4−11 cells was assessed by (J) Annexin V-APC/7-AAD double staining and (K) JC-1 fluorescence. (L) Schematic illustration of the mitochondrial apoptosis pathway activated by TM-VS.

and M-VS showed antagonistic effects at high VEN/SOR ratios of above 4.8/1 (Table S3). M-$VS_{1/4}$ had the best synergistic effect, with IC_{50} values of 0.61 ng/mL (VEN) and 2.42 ng/mL (SOR), which were 63.2- and 4.0-fold lower than those of M-V (VEN: 38.58 ng/mL) and M-S (SOR: 9.61 ng/mL), respectively. In MOLM-13-Luc cells, M-VS with VEN/SOR ratios ranging from 1/1 to 1/6 exhibited strong synergy, with CI values less than 0.1, and M-$VS_{1/2}$ had the most synergistic anti-AML effect, with IC_{50} values as low as 0.16 ng/mL (VEN) and 0.32 ng/mL (SOR) (Figure 3B and Table 2). The CI-Fa curves simulated by CompuSyn software further verified the strong synergy of M-VS in both MV4−11 and MOLM-13-Luc cells (Figure 3C,D).

TM-VS with the optimal drug ratio and T22 peptide density (20%) was then utilized to enable targeted inhibitor delivery and augment the anti-AML effect. TM-$VS_{1/4}$ was 2.4- and 3.2-fold more potent (IC_{50}: 0.24_{VEN} + 0.96_{SOR} ng/mL) against MV4−11 cells than M-$VS_{1/4}$ and free $VS_{1/4}$, respectively (Figure 3E). Similarly, TM-$VS_{1/2}$ exhibited a superior inhibitory effect (IC_{50}: 0.096_{VEN} + 0.192_{SOR} ng/mL) on MOLM-13-Luc cells, which was 2.2- and 2.6-fold greater than that of M-$VS_{1/2}$ and free $VS_{1/2}$, respectively (Figure 3F). Notably, TM-$VS_{1/4}$ and M-$VS_{1/4}$ were nontoxic to normal cells, such as human PBMCs, mouse DC 2.4 cells and mouse L929 fibroblasts, even at VEN/SOR concentrations of 250/1000 ng/mL (Figure 3G and Figure S3), indicating that TM-VS and M-VS loaded with molecular targeted drugs can specifically target cancer cells but spare normal cells. In addition, blank micelles (TM and M) were nontoxic to MV4−11 and MOLM-13-Luc cells at micelle concentrations up to 400 μg/mL (Figure S4).

https://doi.org/10.1021/acs.biomac.4c00561
Biomacromolecules 2024, 25, 4569−4580

Table 2. Summary of the IC_{50} and CI Values of M-VS at Different Drug Ratios in MV4-11 and MOLM-13-Luc Cells

		IC_{50} (ng/mL)		
cell type	samples	VEN	SOR	CI[a]
MV4−11	$M\text{-}VS_{1/1}$	4.84	4.84	0.63
	$M\text{-}VS_{1/2}$	3.05	6.10	0.71
	$M\text{-}VS_{1/4}$	0.61	2.42	0.27
	$M\text{-}VS_{1/6}$	0.74	4.42	0.48
	M-V	38.58		
	M-S		9.61	
MOLM-13-Luc	$M\text{-}VS_{1/1}$	0.34	0.34	0.09
	$M\text{-}VS_{1/2}$	0.16	0.32	0.07
	$M\text{-}VS_{1/4}$	0.10	0.40	0.08
	$M\text{-}VS_{1/6}$	0.07	0.41	0.08
	M-V	12.00		
	M-S		5.28	

[a]Calculated from the synergy formula in section 2.5.

Many AML patients express high levels of the antiapoptotic proteins BCL-2 and MCL-1, especially upon relapse after chemotherapy.[41,42] Bioinformatics analysis based on the TCGA and GTEx databases demonstrated that the antiapoptotic genes BCL-2, MCL-1, and BCL-XL were significantly overexpressed in AML patients (n = 152) compared to healthy people (n = 337) (Figure 3H). Western blot analyses revealed that BCL-2, MCL-1, and BCL-XL proteins were overexpressed in the MV4−11 and MOLM-13-Luc AML cells (Figure 3I). TM-VS treatment efficiently downregulated MCL-1 and BCL-XL expression, resulting in lower protein levels than those of M-VS, free VS, and the single inhibitor formulations (M-S and M-V). The expression of the BCL-2 protein changed little because of the direct binding of VEN to the hydrophobic groove of the BCL-2 protein, which prevented the interaction of BCL-2 protein with pro-apoptotic proteins and resulted in the activation of apoptosis.[43] It has been reported that the combination of a BCL-2 inhibitor and a FLT3 inhibitor can activate the mitochondrial apoptotic pathway through combined inhibition of the antiapoptotic proteins BCL-2, BCL-XL, and MCL-1.[20,44,45]

The proapoptotic ability of the different formulations was evaluated by an Annexin V-APC/7-AAD kit and a JC-1 kit. TM-VS induced the most cell apoptosis in MV4−11 cells, with a total apoptosis rate of 36.2%, which was greater than that of M-VS (27.1%), free VS (26.5%), M-S (19.1%), and M-V (9.9%) (Figure 3J). The loss of mitochondrial membrane potential is an essential indicator of mitochondria-mediated early apoptosis.[45] Figure 3K shows the excellent early

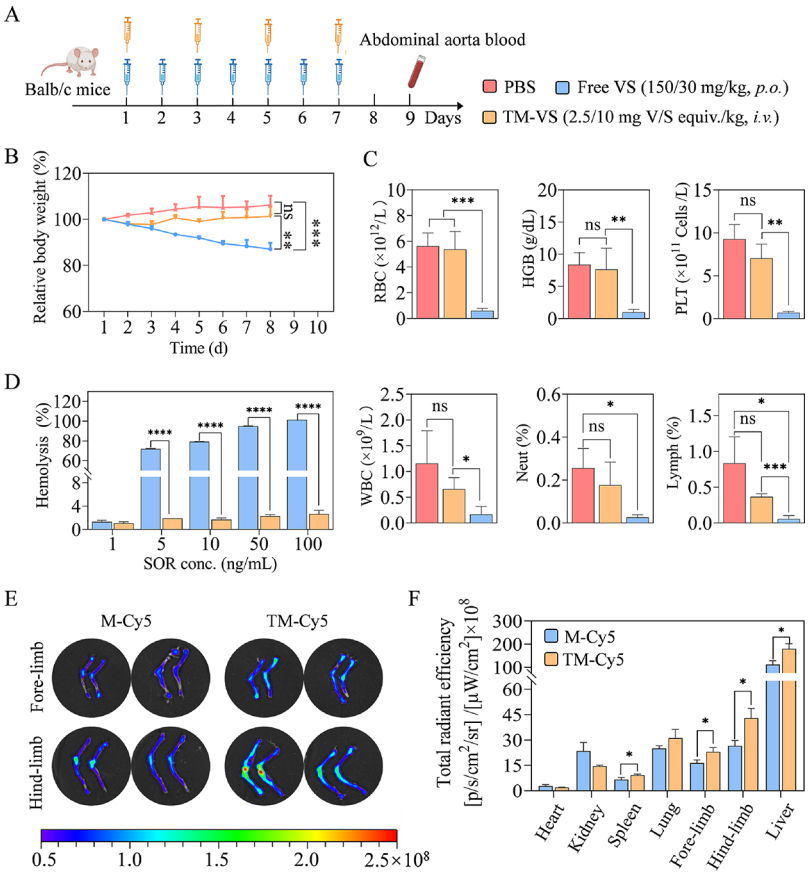

Figure 4. Acute toxicity, hemolysis and biodistribution studies. (A) Schematic illustration of the drug administration schedule for the acute toxicity study. (B) Body weight changes (n = 4) and (C) routine blood analyses of mice injected with free VS, TM-VS or PBS (WBC: white blood cell; RBC: red blood cell; HGB: hemoglobin; PLT: platelet; Neut: neutrophil; Lymph: lymphocyte) (n = 3). (D) Hemolysis rates of erythrocytes after 3 h of incubation with free VS or TM-VS at various drug concentrations at 37 °C and 200 rpm (n = 4, V/S weight ratio was 1/4). Erythrocytes treated with PBS or 1% Triton-X 100 served as negative and positive controls, respectively. (E) Ex vivo Cy5 fluorescence images of the hind and fore limbs and (F) quantitative fluorescence analyses of major organs and hind/fore limbs from orthotopic MV4−11 tumor-bearing mice at 8 h after the injection of TM-Cy5 or M-Cy5 (n = 3). The concentration of Cy5 was 2.5 μg/mL.

https://doi.org/10.1021/acs.biomac.4c00561
Biomacromolecules 2024, 25, 4569−4580

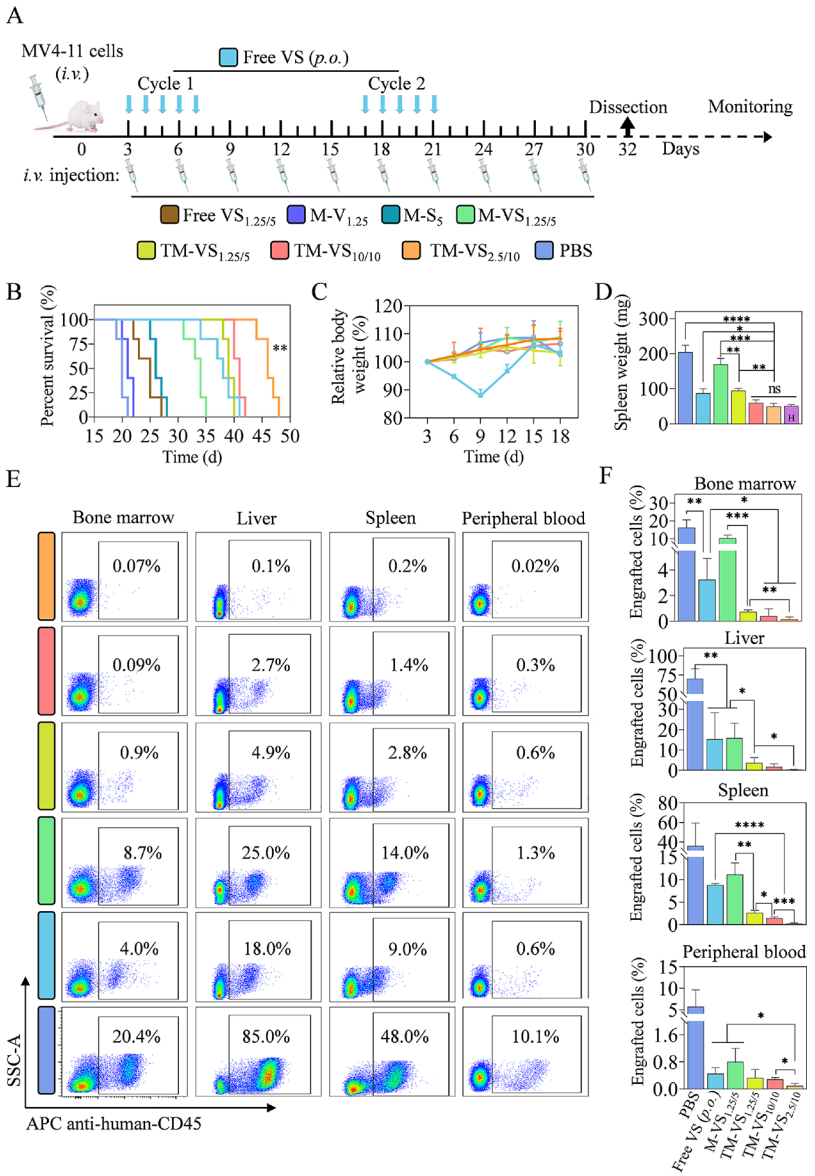

Figure 5. *In vivo* anti-AML efficacy of TM-VS in orthotopic MV4−11 AML-bearing mice (n = 9). (A) Schematic illustration of the treatment schedule. (B) Kaplan−Meier survival curves (TM-$VS_{2.5/10}$ versus all other groups, $^{**}p < 0.01$) and (C) body weight changes of mice following different treatments (n = 5). (D) Weights of spleens isolated from mice in different treatment groups (n = 4). H refers to healthy mice. (E) Representative scatter plot and (F) quantitative analysis of MV4−11 cell infiltration in the bone marrow, liver, spleen, and peripheral blood of mice in different treatment groups (n = 3).

apoptotic ability of TM-VS (early apoptosis rate: 90.7%) in MV4−11 cells. Similarly, TM-VS also exhibited a strong proapoptotic effect on MOLM-13-Luc cells (Figure S5). Collectively, these results confirm that TM-VS can specifically target $CXCR4^+$ AML cells, inhibit the antiapoptotic protein BCL-2, and downregulate MCL-1 and BCL-XL, leading to increased cell apoptosis and enhanced tumor cell growth inhibition (Figure 3L).

3.4. In Vivo Acute Toxicity, Hemolysis, and Biodistribution. Female BALB/c mice (healthy mice) were used to evaluate the acute toxicity of TM-VS and free VS *in vivo* (n = 4). TM-VS (2.5/10 mg V/S equiv/kg) was administered intravenously once every 2 days for a total of 4 injections, and free VS (150/30 mg/kg) was administered orally every day via gavage for 7 days (Figure 4A). PBS was used as a control. The results showed that TM-VS-treated mice maintained a steady weight during administration, approaching that of healthy mice (Figure 4B). However, mice dosed with free VS suffered continued weight loss (15% on day 8), accompanied by obvious adverse effects such as loss of hair and appetite, darkening of fur, and weakness of the hind limbs. Routine blood tests showed that TM-VS-treated mice had blood cell counts comparable to those of healthy mice, while mice in the free VS group exhibited significant abnormalities in all parameters (Figure 4C). Stacking toxicity is one of the main challenges of combination therapies, and nanosystems enable more precise control of drug release and reduce systemic side effects.[46] TM-VS significantly reduced hemolysis to less than 5% at SOR concentrations ranging from 1 to 100 μg/mL, which was in sharp contrast to free VS ($^{****}p < 0.0001$) bearing a rate up to 100% (Figure 4D). The encapsulation of inhibitors by TM significantly improved drug hemocompatibility, which is in line with the results of other studies,[43,47] and offers the potential for intravenous administration of

https://doi.org/10.1021/acs.biomac.4c00561
Biomacromolecules 2024, 25, 4569−4580

combination therapies. To further investigate the *in vivo* performance of TM-VS, an orthotopic MV4−11 AML model was established by tail vein injection of MV4−11 cells (5×10^5) into NSG mice, similar to our previous reports.[48] Ex vivo imaging revealed that TM-Cy5 efficiently accumulated in the hind/fore-limbs, liver, and spleen of mice where the leukemia cells highly enriched, at 8 h after *i.v.* injection, as indicated by the significantly stronger Cy5 fluorescence in the TM-Cy5-injected mice than in the M-Cy5-injected mice (Figure 4E,F). These results demonstrated that compared with the free drug combination, TM-VS minimized weight loss and hematologic toxicity while increasing drug enrichment in the bones, liver, and spleen with high leukemia burden.

3.5. In Vivo Therapeutic Effect of TM-VS in an Orthotopic MV4−11 AML Mouse Model. An orthotopic MV4−11 AML model was established to evaluate the anti-AML activity of TM-VS at different drug ratios and dosages. On day 3 post inoculation of MV4−11 cells, the mice were randomly divided into groups to receive TM-VS at V/S dosages of 1.25/5, 2.5/10, and 10/10 mg/kg, denoted as TM-$V/S_{1.25/5}$, TM-$V/S_{2.5/10}$, and TM-$V/S_{10/10}$, respectively, via intravenous injection (*i.v.*) (Figure 5A). Mice administered with M-$VS_{1.25/5}$, M-$V_{1.25}$, M-S_5, or free $VS_{1.25/5}$ at a V/S dosage of 1.25/5 mg/kg (*i.v.*), free VS (*p.o.*) at a V/S dosage of 150/30 mg/kg, or PBS served as controls. The results showed that the MV4−11 AML model was quite aggressive, with a short median survival time (MST) of 20 days in the PBS group (Figure 5B). After treatment with M-$VS_{1.25/5}$, the MST of the mice was prolonged to 34 days, which was significantly better than that of the M-S_5 (26 days), M-$V_{1.25}$ (21 days), and free $VS_{1.25/5}$ (25 days) groups. In comparison to M-$VS_{1.25/5}$, TM-$VS_{1.25/5}$ at the same dosage further significantly extended mouse survival, with an MST of 39 days (**p), supporting the targetability of TM-VS to $CXCR4^+$ MV4−11 cells. Interestingly, TM-$VS_{2.5/10}$ at a higher dosage further prolonged the MST of the mice to 46 days (**p). Notably, after treatment with TM-$VS_{10/10}$ at a dosage of 10/10 mg V/S equiv/kg, mice only reached a median survival of 41 days, revealing the importance of maintaining an optimal drug weight ratio of 1/4. It should further be noted that free VS (*p.o.*) at a high dosage of 150/30 mg/kg, though extending the MST of mice to 38 days, was inferior to TM-$VS_{2.5/10}$ (**p) and caused severe loss of mouse weight (~13%) as well as darkened fur (Figure 5C). Free $VS_{1.25/5}$ (*i.v.*) also induced mouse shivering, which usually needed 1−2 min to be relieved. In sharp contrast, TM-VS at different dosages and M-VS were well tolerated in mice, showing a steady weight increase, likely due to the shielding of the systemic toxicity of VEN and SOR via micelle encapsulation.

Leukemia cells often infiltrate the spleen, causing splenomegaly, a typical feature of AML.[49,50] Consistent with the survival data, the spleen weights of mice treated with TM-$VS_{2.5/10}$ and TM-$VS_{10/10}$ were similar to those of healthy mice on day 32, in significant contrast to those of the M-$VS_{1.25/5}$ (***p), TM-$VS_{1.25/5}$ (**p), free VS (*p.o.*) (*p), and PBS (****p) groups with massive splenomegaly (Figure 5D). The leukemia infiltration data further provided evidence that TM-$VS_{2.5/10}$ had negligible leukemia blasts in the bone marrow (0.07%), liver (0.1%), spleen (0.2%), and peripheral blood (0.02%), which were more than 30-fold lower than those of free VS (*p.o.*) (4.0%, 18.0%, 9.0%, and 0.6%, respectively) and lower than those of TM-$VS_{10/10}$ (Figure 5E,F). In comparison with M-$VS_{1.25/5}$, TM-$VS_{1.25/5}$ significantly reduced leukemia engraftment in the bone marrow, liver, and spleen, likely due to its ability to target AML cells and its high accumulation in the bone marrow. Notably, highly efficient inhibition of leukemic cells in the bone marrow ecotone is particularly important, as most anti-AML therapies have failed due to difficulties accessing the bone marrow.[51,52]

H&E-stained images further confirmed that TM-VS treatment not only inhibited leukemia infiltration in the bone marrow, spleen, and liver but also caused no obvious damage to the major organs (Figure 6A and Figure S6). This is in

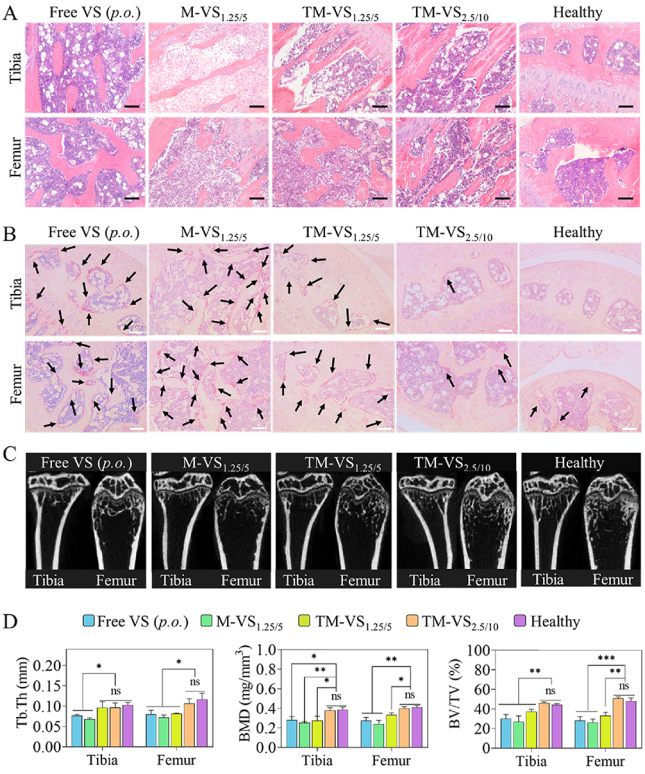

Figure 6. Analysis of the tibias and femurs of orthotopic MV4−11 AML-bearing mice in different treatment groups. Healthy mice were used as controls. (A) H&E-stained images. Scale bars: 100 μm. (B) TRAP-stained images for identifying osteoclasts (crimson). Scale bars: 100 μm. (C) Micro-CT images. (D) Quantitative analysis of the trabecular thickness (Tb.Th), bone mineral density (BMD), and bone volume fraction (BV/TV) (n = 3).

contrast to the M-$VS_{1.25/5}$ group, which exhibited distinct leukemia infiltration, and free VS (*p.o.*) group, which exhibited hemorrhage in the spleen, demonstrating the efficacy and safety of TM-VS. As shown in Figure 6A, the femurs and tibias of mice receiving TM-$VS_{2.5/10}$ possessed similar hematopoietic cells and bone histomorphology to those of healthy mice, in sharp contrast to those of M-$VS_{1.25/5}$-treated mice, which exhibited obvious leukemia infiltration and a reduction in hematopoietic cells. The free VS (*p.o.*) group, in which the mice were treated with a high dose, still exhibited visible tumor infiltration in the bone marrow. The progression of AML cells in the bone marrow is reported to activate osteoclasts, resulting in osteopenia/osteoporosis.[53] TRAP is known as a key marker of osteoclasts.[54] TRAP-stained images showed that the numbers of osteoclasts in the femurs and tibias of mice treated with TM-$VS_{2.5/10}$ were similar to those in healthy mice and significantly lower than those in the free VS (*p.o.*), M-$VS_{1.25/5}$, and TM-$VS_{1.25/5}$ groups (Figure 6B). Micro-CT

https://doi.org/10.1021/acs.biomac.4c00561
Biomacromolecules 2024, 25, 4569−4580

analysis revealed that the tibia and femur of TM-$VS_{2.5/10}$-treated mice had a normal bone structure and comparable trabecular thickness (Tb.Th), bone mineral density (BMD), and bone volume fraction (BV/TV) parameters to those of healthy mice, which were significantly greater than those of the other groups (Figure 6C,D). The progression of AML causes severe suppression of hematopoiesis and an imbalance in the number of blood cells.[55] Routine blood analysis of mice treated with TM-$VS_{2.5/10}$ or TM-$VS_{10/10}$ had similar levels of erythrocytes, platelets, hemoglobin, and neutrophils to healthy mice (Figure S7), revealing the low systemic toxicity and AML burden. However, free VS (*p.o.*)-treated mice presented significantly lower levels of blood cells, which may be caused by stacking toxicity of dual drugs.

4. CONCLUSIONS

We have demonstrated that CXCR4-mediated targeted codelivery of clinically used BCL-2 and FLT3 inhibitors, venetoclax and sorafenib, achieves strong synergetic therapy of orthotopic FLT3-ITD AML in mice. Notably, dual inhibitor-loaded micelles at the optimum drug ratio have not only markedly reduced the drug dosage and thereby relieved the side effects but also greatly improved the therapeutic effect, leading to significantly prolonged median survival time of MV4−11 AML-bearing mice. This dual-inhibitor nanoformulation (TM-VS) exhibit many favorable properties such as small size of about 40 nm, stable drug encapsulation, and redox-responsive release of both drugs. The targeted nanodelivery of BCL-2 and FLT3 inhibitors offers a potential treatment strategy for FLT3-ITD AML patients and warrants further investigation.

■ ASSOCIATED CONTENT

Supporting Information

The Supporting Information is available free of charge at https://pubs.acs.org/doi/10.1021/acs.biomac.4c00561.

Details on materials, cell culture, animals, and characterizations; experiment details on the synthesis of copolymers, in vitro drug release, CLSM, and hemolysis studies; tables showing characterization of copolymers and single inhibitor loaded micelles as well as IC_{50} and CI values of M-VS at high VEN-to-SOR ratios in MV4−11 cells; scheme showing the preparation of TM-VS; synthetic route of T22-PEG-*b*-P(CL-*co*-DTC) copolymer; figures showing ^{1}H NMR spectra of copolymers; cytotoxicity of M-VS against PBMCs, DC 2.4 cells, and L929 cells; cytotoxicity of targeted and nontargeted blank micelles (TM and M) against AML cells; cell apoptosis of MOLM-13-Luc cells; H&E-stained images of major organs; blood routine parameters of mice in different treatment groups (PDF)

■ AUTHOR INFORMATION

Corresponding Authors

Ru Cheng − *Biomedical Polymers Laboratory, College of Chemistry, Chemical Engineering and Materials Science, and State Key Laboratory of Radiation Medicine and Protection and Soochow College, Soochow University, Suzhou 215123, P. R. China;* orcid.org/0000-0002-0879-5069; Phone: +86-512-65880098; Email: rcheng@suda.edu.cn

Huanli Sun − *Biomedical Polymers Laboratory, College of Chemistry, Chemical Engineering and Materials Science, and State Key Laboratory of Radiation Medicine and Protection, Soochow University, Suzhou 215123, P. R. China;* orcid.org/0000-0001-6287-1555; Email: huanli@suda.edu.cn

Zhiyuan Zhong − *Biomedical Polymers Laboratory, College of Chemistry, Chemical Engineering and Materials Science, and State Key Laboratory of Radiation Medicine and Protection and College of Pharmaceutical Sciences, Soochow University, Suzhou 215123, P. R. China;* orcid.org/0000-0003-4175-4741; Email: zyzhong@suda.edu.cn

Authors

Jiakun Yang − *Biomedical Polymers Laboratory, College of Chemistry, Chemical Engineering and Materials Science, and State Key Laboratory of Radiation Medicine and Protection, Soochow University, Suzhou 215123, P. R. China*

Peng Zhang − *Biomedical Polymers Laboratory, College of Chemistry, Chemical Engineering and Materials Science, and State Key Laboratory of Radiation Medicine and Protection, Soochow University, Suzhou 215123, P. R. China*

Yumin Mao − *Biomedical Polymers Laboratory, College of Chemistry, Chemical Engineering and Materials Science, and State Key Laboratory of Radiation Medicine and Protection, Soochow University, Suzhou 215123, P. R. China*

Ran Chen − *Biomedical Polymers Laboratory, College of Chemistry, Chemical Engineering and Materials Science, and State Key Laboratory of Radiation Medicine and Protection, Soochow University, Suzhou 215123, P. R. China*

Jiaying Li − *Orthopedic Institute, Soochow University, Suzhou 215007, PR China*

Chao Deng − *Biomedical Polymers Laboratory, College of Chemistry, Chemical Engineering and Materials Science, and State Key Laboratory of Radiation Medicine and Protection, Soochow University, Suzhou 215123, P. R. China;* orcid.org/0000-0001-7697-9874

Complete contact information is available at: https://pubs.acs.org/10.1021/acs.biomac.4c00561

Author Contributions

The manuscript was written through contributions of all authors. All authors have given approval to the final version of the manuscript.

Notes

The authors declare no competing financial interest.

■ ACKNOWLEDGMENTS

This work is supported by research grants from the National Natural Science Foundation of China (NSFC 52073195, 51873144 and 52073196), the Natural Science Foundation of the Jiangsu Higher Education Institutions of China (21KJA150007), and the Qinglan Program of the Jiangsu Higher Education Institutions.

■ REFERENCES

(1) DiNardo, C. D.; Erba, H. P.; Freeman, S. D.; Wei, A. H. Acute myeloid leukemia. *Lancet* **2023**, *401* (10393), 2073−2086.

(2) Kantarjian, H.; Kadia, T.; DiNardo, C.; Daver, N.; Borthakur, G.; Jabbour, E.; Garcia-Manero, G.; Konopleva, M.; Ravandi, F. Acute myeloid leukemia: current progress and future directions. *Blood Cancer J.* **2021**, *11* (2), 41−66.

(3) Döhner, H.; Weisdorf, D. J.; Bloomfield, C. D. Acute myeloid leukemia. *N. Engl. J. Med.* **2015**, *373* (12), 1136−1152.

(4) Bhansali, R. S.; Pratz, K. W.; Lai, C. Recent advances in targeted therapies in acute myeloid leukemia. *J. Hematol. Oncol.* **2023**, *16* (1), 29−56.
(5) Shimony, S.; Stahl, M.; Stone, R. M. Acute myeloid leukemia: 2023 update on diagnosis, risk stratification, and management. *Am. J. Hematol.* **2023**, *98* (3), 502−526.
(6) Yue, S.; An, J.; Zhang, Y.; Li, J.; Zhao, C.; Liu, J.; Liang, L.; Sun, H.; Xu, Y.; Zhong, Z. Exogenous antigen upregulation empowers antibody targeted nanochemotherapy of leukemia. *Adv. Mater.* **2023**, *35*, 2209984.
(7) Ley, T. J.; Mardis, E. R.; Ding, L.; Fulton, B.; McLellan, M. D.; Chen, K.; Dooling, D.; Dunford-Shore, B. H.; McGrath, S.; Hickenbotham, M.; Cook, L.; Abbott, R.; Larson, D. E.; Koboldt, D. C.; Pohl, C.; Smith, S.; Hawkins, A.; Abbott, S.; Locke, D.; Hillier, L. W.; Miner, T.; Fulton, L.; Magrini, V.; Wylie, T.; Glasscock, J.; Conyers, J.; Sander, N.; Shi, X.; Osborne, J. R.; Minx, P.; Gordon, D.; Chinwalla, A.; Zhao, Y.; Ries, R. E.; Payton, J. E.; Westervelt, P.; Tomasson, M. H.; Watson, M.; Baty, J.; Ivanovich, J.; Heath, S.; Shannon, W. D.; Nagarajan, R.; Walter, M. J.; Link, D. C.; Graubert, T. A.; DiPersio, J. F.; Wilson, R. K. DNA sequencing of a cytogenetically normal acute myeloid leukemia genome. *Nature* **2008**, *456* (7218), 66−72.
(8) Ediriwickrema, A.; Gentles, A. J.; Majeti, R. Single-cell genomics in AML: Extending the frontiers of AML research. *Blood* **2023**, *141* (4), 345−355.
(9) Kayser, S.; Levis, M. J. The clinical impact of the molecular landscape of acute myeloid leukemia. *Haematologica* **2023**, *108* (2), 308−320.
(10) Van Galen, P.; Hovestadt, V.; Wadsworth, M. H., II; Hughes, T. K.; Griffin, G. K.; Battaglia, S.; Verga, J. A.; Stephansky, J.; Pastika, T. J.; Story, J. L. Single-cell RNA-seq reveals AML hierarchies relevant to disease progression and immunity. *Cell* **2019**, *176* (6), 1265−1281, DOI: 10.1016/j.cell.2019.01.031.
(11) Zhao, J. C.; Agarwal, S.; Ahmad, H.; Amin, K.; Bewersdorf, J. P.; Zeidan, A. M. A review of FLT3 inhibitors in acute myeloid leukemia. *Blood Rev.* **2022**, *52*, 100905.
(12) Smith, C. C.; Wang, Q.; Chin, C. S.; Salerno, S.; Damon, L. E.; Levis, M. J.; Perl, A. E.; Travers, K. J.; Wang, S.; Hunt, J. P.; Zarrinkar, P. P.; Schadt, E. E.; Kasarskis, A.; Kuriyan, J.; Shah, N. P. Validation of ITD mutations in FLT3 as a therapeutic target in human acute myeloid leukemia. *Nature* **2012**, *485* (7397), 260−263.
(13) Daver, N.; Schlenk, R. F.; Russell, N. H.; Levis, M. J. Targeting FLT3 mutations in AML: review of current knowledge and evidence. *Leukemia* **2019**, *33* (2), 299−312.
(14) Antar, A. I.; Otrock, Z. K.; Jabbour, E.; Mohty, M.; Bazarbachi, A. FLT3 inhibitors in acute myeloid leukemia: ten frequently asked questions. *Leukemia* **2020**, *34* (3), 682−696.
(15) Döhner, H.; Wei, A. H.; Löwenberg, B. Toward precision medicine for AML. *Nat. Rev. Clin. Oncol.* **2021**, *18* (9), 577−590.
(16) Delbridge, A. R.; Grabow, S.; Strasser, A.; Vaux, D. L. Thirty years of BCL-2: translating cell death discoveries into novel cancer therapies. *Nat. Rev. Cancer* **2016**, *16* (2), 99−109.
(17) Konopleva, M.; Letai, A. BCL-2 inhibition in AML: an unexpected bonus? *Blood* **2018**, *132* (10), 1007−1012.
(18) DiNardo, C. D.; Konopleva, M. Y. A venetoclax bench-to-bedside story. *Nat. Cancer* **2021**, *2* (1), 3−5.
(19) El-Cheikh, J.; Bidaoui, G.; Saleh, M.; Moukalled, N.; Abou Dalle, I.; Bazarbachi, A. Venetoclax: a new partner in the novel treatment era for acute myeloid leukemia and myelodysplastic syndrome. *Clin. Hematol. Int.* **2023**, *5* (2), 143−154.
(20) Mali, R. S.; Zhang, Q.; DeFilippis, R. A.; Cavazos, A.; Kuruvilla, V. M.; Raman, J.; Mody, V.; Choo, E. F.; Dail, M.; Shah, N. P. Venetoclax combines synergistically with FLT3 inhibition to effectively target leukemic cells in FLT3-ITD+ acute myeloid leukemia models. *Haematologica* **2021**, *106* (4), 1034−1046.
(21) Zhu, R.; Li, L.; Nguyen, B.; Seo, J.; Wu, M.; Seale, T.; Levis, M.; Duffield, A.; Hu, Y.; Small, D. FLT3 tyrosine kinase inhibitors synergize with BCL-2 inhibition to eliminate FLT3/ITD acute leukemia cells through BIM activation. *Signal Transduction Targeted Ther.* **2021**, *6* (1), 186−197.
(22) Moses, B. S.; McCullough, S.; Fox, J. M.; Mott, B. T.; Bentzen, S. M.; Kim, M.; Tyner, J. W.; Lapidus, R. G.; Emadi, A.; Rudek, M. A.; Kingsbury, T. J.; Civin, C. I. Antileukemic efficacy of a potent artemisinin combined with sorafenib and venetoclax. *Blood Adv.* **2021**, *5* (3), 711−724.
(23) Diepstraten, S. T.; Anderson, M. A.; Czabotar, P. E.; Lessene, G.; Strasser, A.; Kelly, G. L. The manipulation of apoptosis for cancer therapy using BH3-mimetic drugs. *Nat. Rev. Cancer* **2022**, *22* (1), 45−64.
(24) Milnerowicz, S.; Maszewska, J.; Skowera, P.; Stelmach, M.; Lejman, M. AML under the scope: current strategies and treatment involving FLT3 inhibitors and venetoclax-based regimens. *Int. J. Mol. Sci.* **2023**, *24* (21), 15849−15873.
(25) Short, N. J.; Nguyen, D.; Ravandi, F. Treatment of older adults with FLT3-mutated AML: Emerging paradigms and the role of frontline FLT3 inhibitors. *Blood Cancer J.* **2023**, *13* (1), 142−151.
(26) Daver, N.; Perl, A. E.; Maly, J.; Levis, M.; Ritchie, E.; Litzow, M.; McCloskey, J.; Smith, C. C.; Schiller, G.; Bradley, T.; Tiu, R. V.; Naqvi, K.; Dail, M.; Brackman, D.; Siddani, S.; Wang, J.; Chyla, B.; Lee, P.; Altman, J. K. Venetoclax plus gilteritinib for FLT3-mutated relapsed/refractory acute myeloid leukemia. *J. Clin. Oncol.* **2022**, *40* (35), 4048−4059.
(27) Du, W.; Lu, C.; Zhu, X.; Hu, D.; Chen, X.; Li, J.; Liu, W.; Zhu, J.; He, Y.; Yao, J. Prognostic significance of CXCR4 expression in acute myeloid leukemia. *Cancer Med.* **2019**, *8* (15), 6595−6603.
(28) Kim, M. Y. CXCR4 to improve both T cell homing and function. *Blood* **2023**, *141* (21), 2546−2547.
(29) Pallarès, V.; Núñez, Y.; Sánchez-García, L.; Falgàs, A.; Serna, N.; Unzueta, U.; Gallardo, A.; Alba-Castellón, L.; Álamo, P.; Sierra, J.; Villaverde, A.; Vázquez, E.; Casanova, I.; Mangues, R. Antineoplastic effect of a diphtheria toxin-based nanoparticle targeting acute myeloid leukemia cells overexpressing CXCR4. *J. Controlled Release* **2021**, *335*, 117−129.
(30) Whiteley, A. E.; Price, T. T.; Cantelli, G.; Sipkins, D. A. Leukaemia: a model metastatic disease. *Nat. Rev. Cancer* **2021**, *21* (7), 461−475.
(31) Burger, J.; Peled, A. CXCR4 antagonists: targeting the microenvironment in leukemia and other cancers. *Leukemia* **2009**, *23* (1), 43−52.
(32) Unzueta, U.; Céspedes, M. V.; Ferrer-Miralles, N.; Casanova, I.; Cedano, J.; Corchero, J. L.; Domingo-Espín, J.; Villaverde, A.; Mangues, R.; Vázquez, E. Intracellular CXCR4^{+} cell targeting with T22-empowered protein-only nanoparticles. *Int. J. Nanomed.* **2012**, *7*, 4533−4544.
(33) Chou, T. C. Theoretical basis, experimental design, and computerized simulation of synergism and antagonism in drug combination studies. *Pharmacol. Rev.* **2006**, *58* (3), 621−681.
(34) Wei, J.; Xia, Y.; Meng, F.; Ni, D.; Qiu, X.; Zhong, Z. Small, smart, and LDLR-specific micelles augment sorafenib therapy of glioblastoma. *Biomacromolecules* **2021**, *22* (11), 4814−4822.
(35) Yang, S.; Zhang, B.; Gong, X.; Wang, T.; Liu, Y.; Zhang, N. *In vivo* biodistribution, biocompatibility, and efficacy of sorafenib-loaded lipid-based nanosuspensions evaluated experimentally in cancer. *Int. J. Nanomed.* **2016**, 2329−2343.
(36) Babos, G.; Biró, E.; Meiczinger, M.; Feczkó, T. Dual drug delivery of sorafenib and doxorubicin from PLGA and PEG-PLGA polymeric nanoparticles. *Polymers* **2018**, *10* (8), 895−907.
(37) Benizri, S.; Ferey, L.; Alies, B.; Mebarek, N.; Vacher, G.; Appavoo, A.; Staedel, C.; Gaudin, K.; Barthélémy, P. Nucleoside-lipid-based nanocarriers for sorafenib delivery. *Nanoscale Res. Lett.* **2018**, *13*, 1−8.
(38) Guo, B.; Qu, Y.; Sun, Y.; Zhao, S.; Yuan, J.; Zhang, P.; Zhong, Z.; Meng, F. Codelivery of gemcitabine and paclitaxel plus NanoCpG empowers chemoimmunotherapy of postoperative "cold" triple-negative breast cancer. *Bioact. Mater.* **2023**, *25*, 61−72.
(39) Gu, W.; An, J.; Meng, H.; Yu, N.; Zhong, Y.; Meng, F.; Xu, Y.; Cornelissen, J. J. L. M.; Zhong, Z. CD44-specific A6 short peptide

boosts targetability and anticancer efficacy of polymersomal epirubicin to orthotopic human multiple myeloma. *Adv. Mater.* **2019**, *31* (46), 1904742.
(40) Wang, Y.; Xie, Y.; Oupický, D. Potential of CXCR4/CXCL12 chemokine axis in cancer drug delivery. *Curr. Pharmacol. Rep.* **2016**, *2*, 1−10.
(41) Kadia, T. M.; Kantarjian, H. M.; Konopleva, M. Myeloid cell leukemia-1 dependence in acute myeloid leukemia: a novel approach to patient therapy. *Oncotarget* **2019**, *10* (12), 1250−1265.
(42) Moon, J. H.; Sohn, S. K.; Lee, M.-H.; Jang, J. H.; Kim, K.; Jung, C. W.; Kim, D. H. BCL2 gene polymorphism could predict the treatment outcomes in acute myeloid leukemia patients. *Leuk. Res.* **2010**, *34* (2), 166−172.
(43) Xie, J.; Zhao, X.; Zhang, P.; Zhang, Y.; Cheng, R.; Zhong, Z.; Deng, C. Codelivery of BCL2 and MCL1 inhibitors enabled by phenylboronic acid-functionalized polypeptide nanovehicles for synergetic and potent therapy of acute myeloid leukemia. *Adv. Sci.* **2023**, *10* (8), 2204866.
(44) Xu, Y.; Ye, H. Progress in understanding the mechanisms of resistance to BCL-2 inhibitors. *Exp. Hematol. Oncol.* **2022**, *11* (1), 1−11.
(45) Carneiro, B. A.; El-Deiry, W. S. Targeting apoptosis in cancer therapy. *Nat. Rev. Clin. Oncol.* **2020**, *17* (7), 395−417.
(46) Mehrotra, N.; Kharbanda, S.; Singh, H. BH3 mimetics in cancer therapy and their future perspectives with nanodelivery. *Nanomedicine* **2021**, *16* (13), 1067−1070.
(47) Bala Tannan, N.; Manzari, M. T.; Herviou, L.; Da Silva Ferreira, M.; Hagen, C.; Kiguchi, H.; Manova-Todorova, K.; Seshan, V.; de Stanchina, E.; Heller, D. A. Tumor-targeted nanoparticles improve the therapeutic index of BCL-2 and MCL-1 dual inhibition. *Blood* **2021**, *137* (15), 2057−2069.
(48) Du, J.; Yue, S.; Li, C.; Li, J.; Zhao, S.; Dong, Y.; Zhang, Y.; Cheng, R.; Sun, H.; Zhong, Z. Exogenous CD38 upregulation enables high-efficacy dually cascade targeted molecular therapy of leukemia. *Nano Today* **2023**, *50*, No. 101872.
(49) Chang, H.; Brandwein, J.; Chun, K.; Patterson, B.; Brien, B. Extramedullary infiltrates of AML are associated with CD56 expression, 11q23 abnormalities and inferior clinical outcome. *Leuk. Res.* **2004**, *28* (10), 1007−1011.
(50) Giagounidis, A.; Burk, M.; Meckenstock, G.; Koch, A.; Schneider, W. Pathologic rupture of the spleen in hematologic malignancies: two additional cases. *Ann. Hematol.* **1996**, *73*, 297−302.
(51) Wang, A.; Zhong, H. Roles of the bone marrow niche in hematopoiesis, leukemogenesis, and chemotherapy resistance in acute myeloid leukemia. *Hematology* **2018**, *23* (10), 729−739.
(52) Bolandi, S. M.; Pakjoo, M.; Beigi, P.; Kiani, M.; Allahgholipour, A.; Goudarzi, N.; Khorashad, J. S.; Eiring, A. M. A role for the bone marrow microenvironment in drug resistance of acute myeloid leukemia. *Cells* **2021**, *10* (11), 2833−2856.
(53) Yuan, B.; Ly, S.; Nguyen, K.; Tran, V.; Maldonado, K.; Kinglsey, C.; Burks, J. K.; Zhou, X.; deCrombrugghe, B.; Andreeff, M.; Battula, V. L. Acute myeloid leukemia expands osteoprogenitor rich niche in the bone marrow but resorbs mature bone causing osteopenia/osteoporosis in animal models. *Blood* **2018**, *132*, 86−97.
(54) Janckila, A. J.; Yam, L. T. Biology and clinical significance of tartrate-resistant acid phosphatases: new perspectives on an old enzyme. *Calcif. Tissue Int.* **2009**, *85*, 465−483.
(55) Khwaja, A.; Bjorkholm, M.; Gale, R. E.; Levine, R. L.; Jordan, C. T.; Ehninger, G.; Bloomfield, C. D.; Estey, E.; Burnett, A.; Cornelissen, J. J. Acute myeloid leukemia. *Nat. Rev. Dis. Primers* **2016**, *2* (1), 1−22.

https://doi.org/10.1021/acs.biomac.4c00561
Biomacromolecules 2024, 25, 4569−4580